Supporting information

Surface in-situ modulation for carbon nanotube-supported Fe-Ni compounds via electrochemical reduction to enhance the catalytic performance for oxygen evolution reaction

Taotao Gao[a], Qi An[a], Yang Zhang[a], Qu Yue[a], Chongbo Liu[a], Xiaoqin Li[a], Bing Li[b], Lu Qiu[a,c*], Dan Xiao[a,c*], Qian Zhao[a*]

a Institute for Advanced Study, School of Mechanical Engineering, Chengdu University, Chengdu, 610106, P. R. China.

E-mail: xiaodan@scu.edu.cn, qiulu@cdu.edu.cn, and zhao_qian@cdu.edu.cn

b Hubei Key Laboratory of Wudang Local Chinese Medicine Research, Hubei University of Medicine, Shiyan, 442000, P. R. China.

c College of Chemical Engineering, Sichuan University, Chengdu, 610065, P. R. China

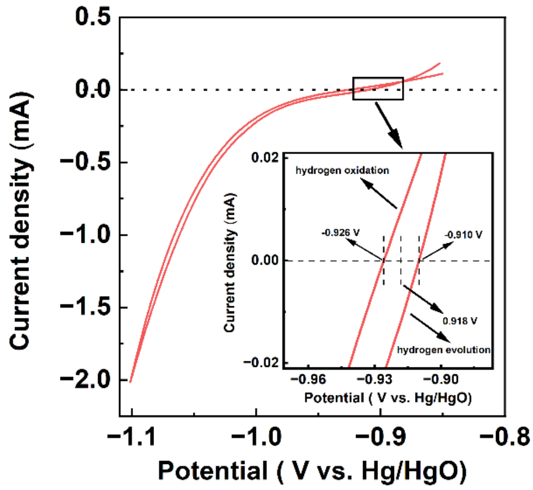

Fig. S1 RHE calibration of Hg/HgO reference electrode.

The correction curve for the Hg/HgO reference electrode is shown in Fig. S1. The calibration is carried out in the 1 M KOH electrolyte with a Pt plate and a carbon rod as the working electrode and counter electrode, respectively. Cyclic voltammetry is conducted at a scan rate of 10 mV s^{-1}, and the average of the two potentials at which the current crossed zero is taken as the thermodynamic potential for the reversible hydrogen electrode.[1] In this work, the calibration value is 0.918 V. RHE (Fig. S1, inset).

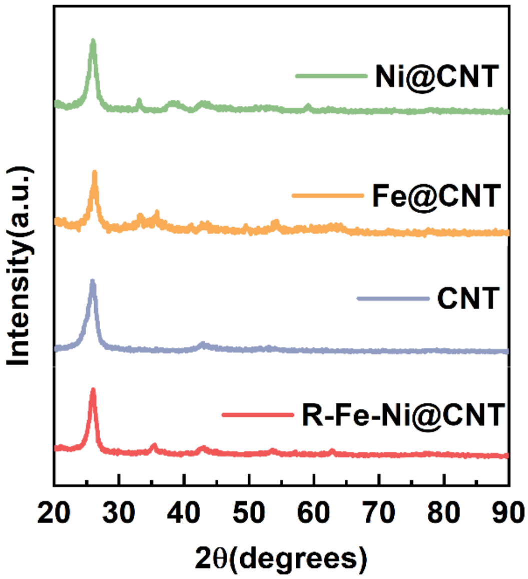

Fig. S2. XRD patterns of the samples.

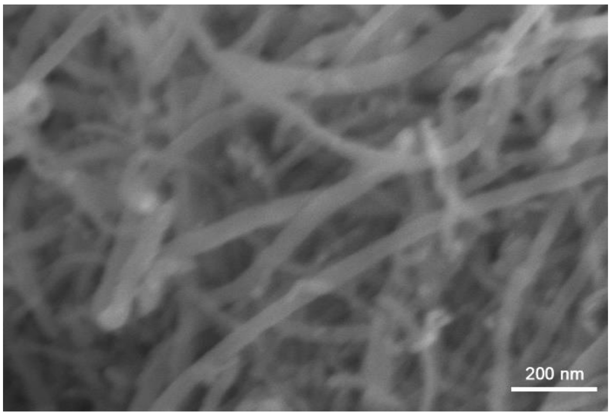

Fig. S3. SEM image of CNT.

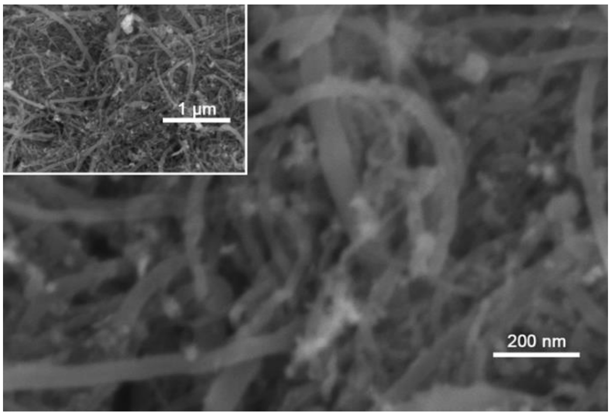

Fig. S4. SEM images of Fe@CNT.

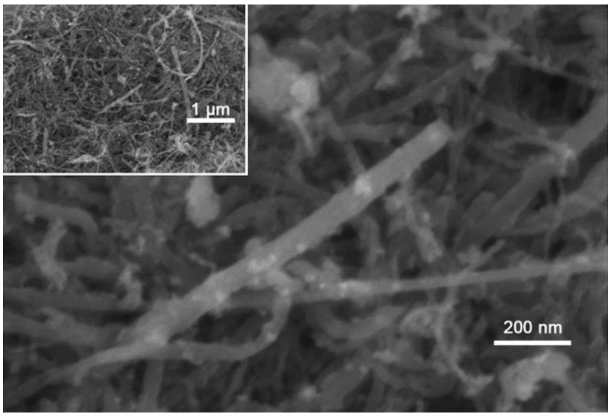

Fig. S5. SEM images of Ni@CNT.

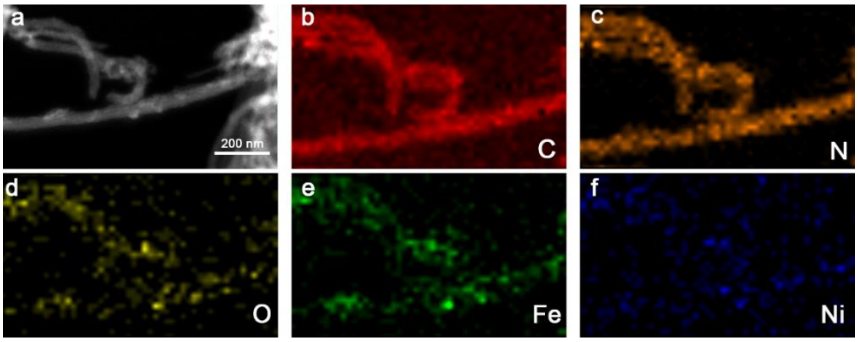

Fig. S6. The TEM mapping images of Fe-Ni@CNT.

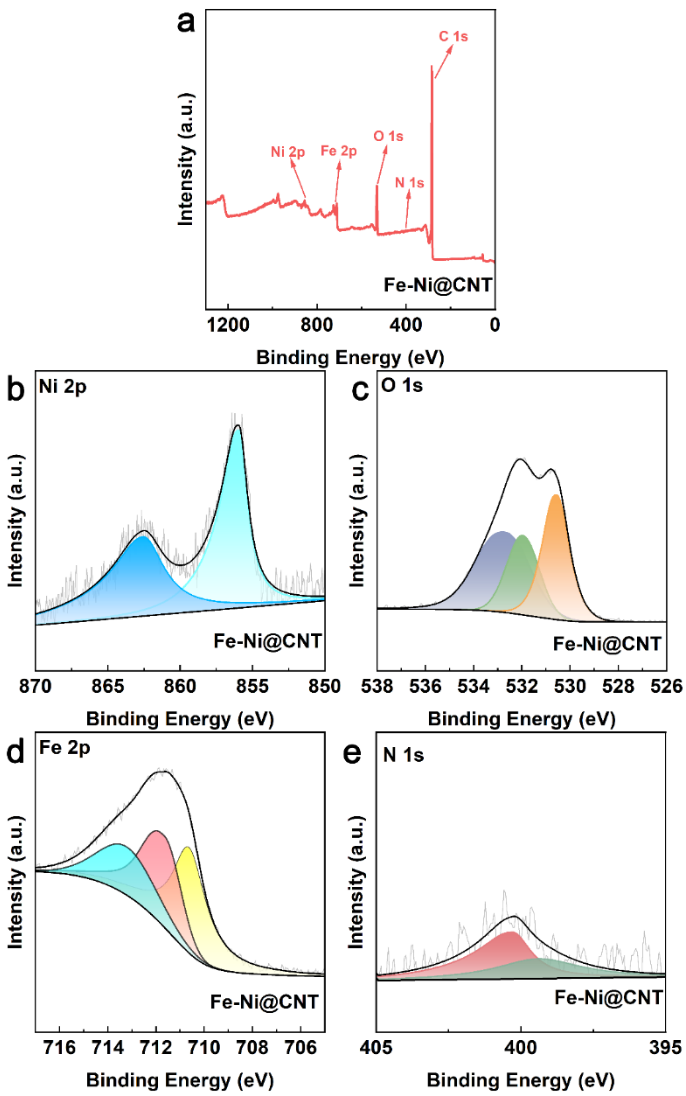

Fig. S7. XPS spectra of the Fe-Ni@CNT.

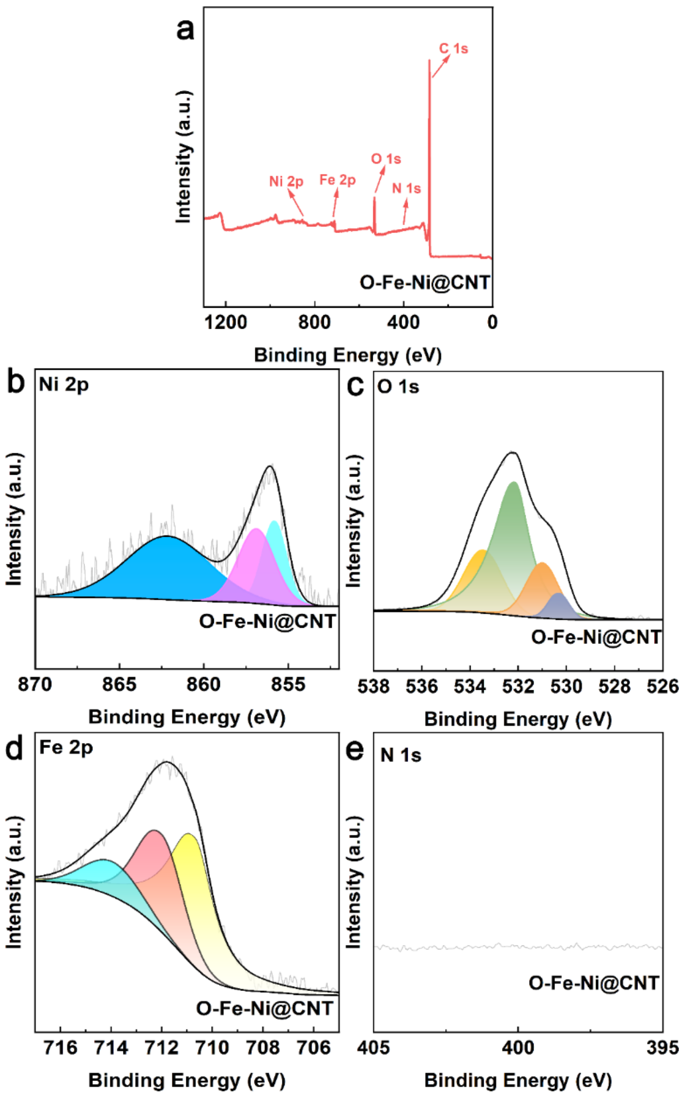

Fig. S8. XPS spectra of the O-Fe-Ni@CNT.

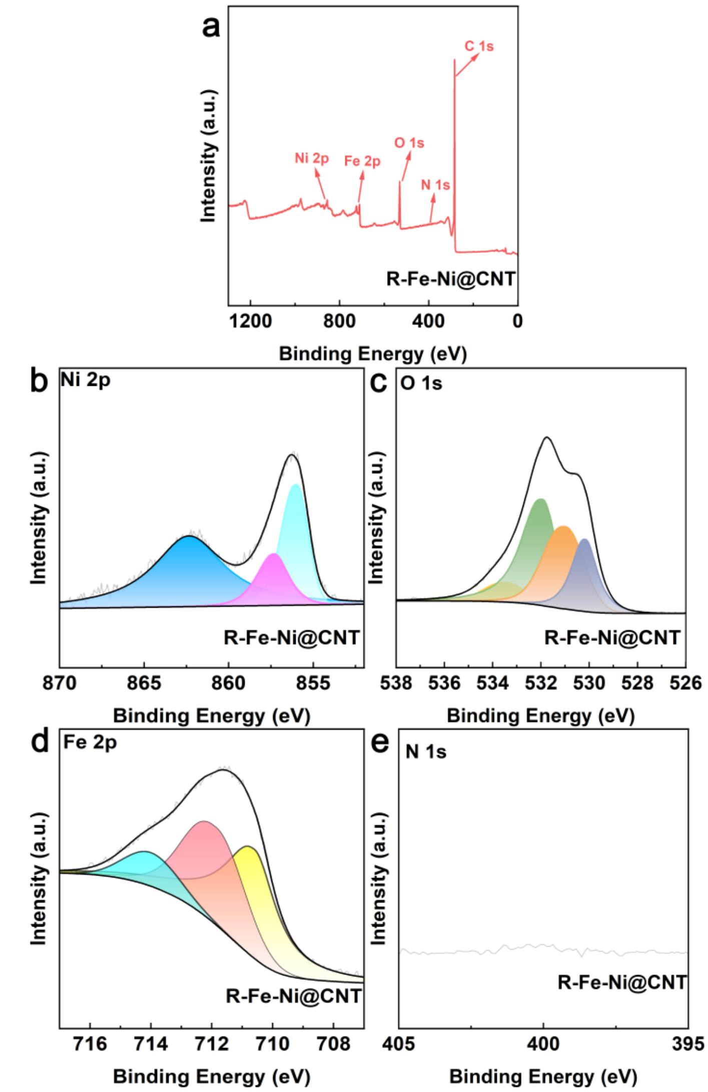

Fig. S9. XPS spectra of the R-Fe-Ni@CNT

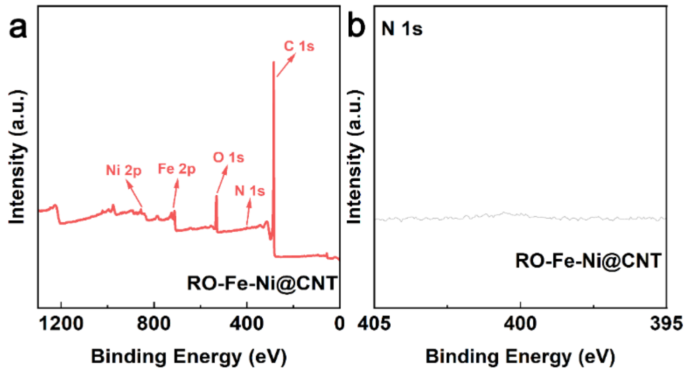

Fig. S10. XPS spectra of the RO-Fe-Ni@CNT.

Table S1. According to the XPS spectra, the proportion of O with different chemical environments in the samples.

	O%			
O Chemical environment	Water	C-O	M-OOH	M-O
Fe-Ni@CNT	36.35	38.85	0	24.8
O-Fe-Ni@CNT	22.63	54.60	17.73	5.04
R-Fe-Ni@CNT	14.55	35.49	22.54	27.42
RO-Fe-Ni@CNT	17.69	28.58	37.13	16.6

Table S2. According to the XPS spectra, the proportion of Ni with different chemical environments in the samples.

	Ni%	
Chemical environment	Ni(2+)	Ni(3+)
Ni@CNT	100	0
Fe-Ni@CNT	100	0
O-Fe-Ni@CNT	41.20	58.80
R-Fe-Ni@CNT	66.49	33.51
RO-Fe-Ni@CNT	30.55	69.45
O-Fe-Ni@CNT (After stability testing)	44.55	55.45
RO-Fe-Ni@CNT (After stability testing)	31.97	68.03

Table S3. Fe and Ni contents were measured by ICP-OES.

Catalysts	Fe	Ni
Fe@CNT	27.47%	-
Ni@CNT	-	7.56%
Fe-Ni@CNT	15.18%	3.68%
O-Fe-Ni@CNT	13.28%	3.01%
R-Fe-Ni@CNT	14.97%	3.54%
RO-Fe-Ni@CNT	14.41%	3.35%

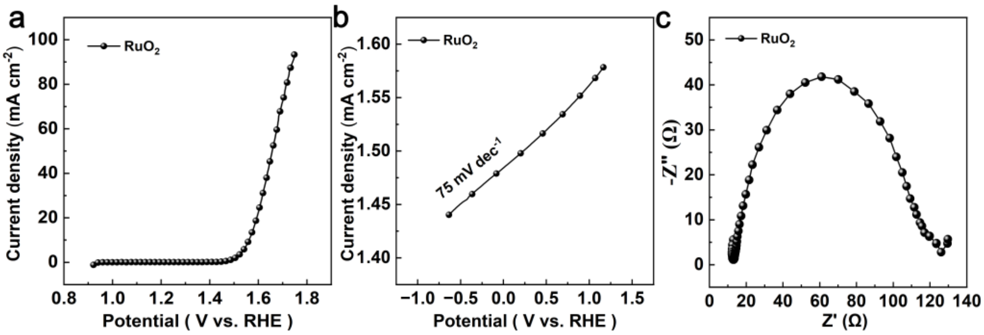

Fig. S11. (a) Polarization curve, (b) Tafel curve, and (c) the electrochemical impedance spectroscopy of RuO_2.

Table S4. Comparison of the OER catalytic activity in 1 M KOH.

Catalysts	Collector	Tafel slope ($mV\ dec^{-1}$)	Overpotential (mV) at different current density ($mA\ cm^{-2}$)			References
			10	100	200	
$Ni_2Fe(O)OH/IF$	Iron foam	51.16	-	245	-	2
$NiCoFe_xP/CC$	Carbon cloth	56	-	~280	~340	3
0.6 wt%-Fe_2O_3@Ni MOF-74	Carbon paper	64	264	~310	~330	4
Ni-Fe LDH hollow prisms	Glassy carbon electrode	49.4	280	~330	-	5
Fe/Ni NWs/NF	Nickel foam	55.8	-	318	~330	6
FeNi-MOF	Rotary disk electrode	49	-	287	~310	7
$FeNi_{4.34}$@FeNi-foil	FeNi-foil	53	283	-	-	8
$Ni/NiFe_2O_4$-CNTsHMS	Rotating disk electrode	46.03	311	-	-	9
$FeNi_2S_4$NPs/CB	Rotating disk electrode	68	290	-	-	10
NiCd(A)Fe	Rotating disk electrode	38	290	-	-	11
$Mn_{0.1}Fe_{0.1}Ni_{0.3}Co_{2.5}O_4$	Glassy carbon electrode	-	362	~410	~450	12
$NiFeO_x(OH)_y$@NCA	Glassy carbon electrode	72	304	-	-	13
RO-Fe-Ni@CNT	Glassy carbon electrode	48	263	316	343	This work
O-Fe-Ni@CNT	Glassy carbon electrode	67	336	-	-	This work

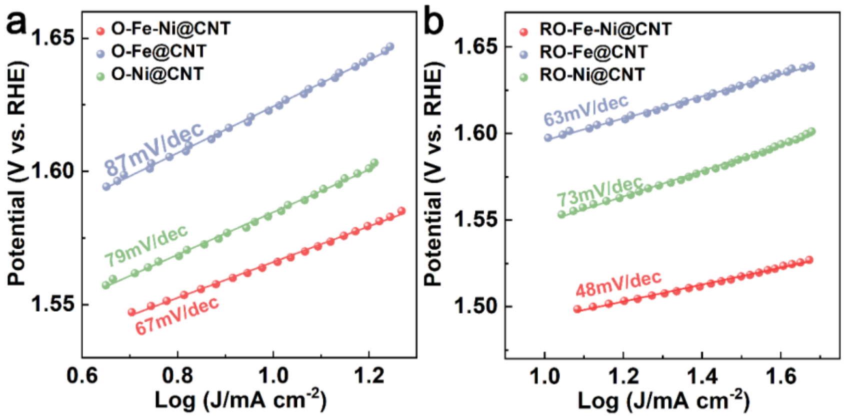

Fig. S12. Tafel curves of (a) O-Fe-Ni@CNT, O-Fe@CNT, O-Ni@CNT and (b) RO-Fe-Ni@CNT, RO-Fe@CNT and RO-Ni@CNT.

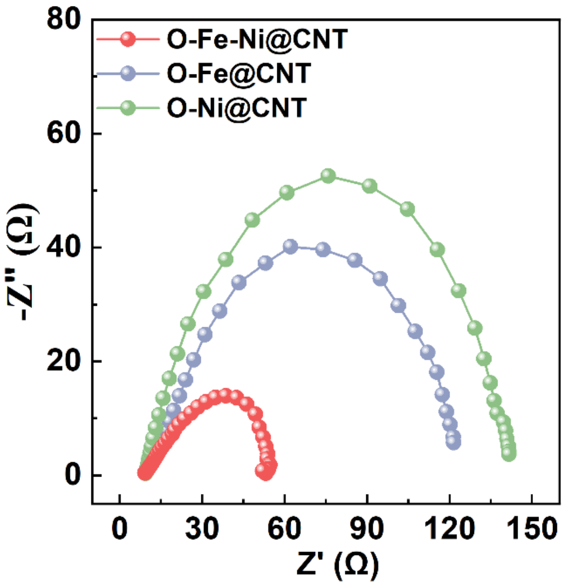

Fig. S13. Electrochemical impedance spectroscopy of O-Fe-Ni@CNT, O-Fe@CNT, and O-Ni@CNT.

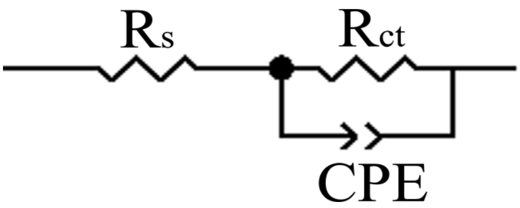

Fig. S14. The equivalent circuit model used to fit Nyquist plots.

Table S5. Charge transfer resistance (R_{ct}) and solution resistance (R_s) of the samples.

Catalysts	R_{ct} (Ω)	R_s (Ω)
O-Fe-Ni@CNT	54.7	9.2
RO-Fe-Ni@CNT	9.3	8.6
O-Ni@CNT	132.0	8.9
RO-Ni@CNT	62.6	8.2
O-Fe@CNT	116.0	9.1
RO-Fe@CNT	49.0	8.7
RuO_2	103.0	9.6

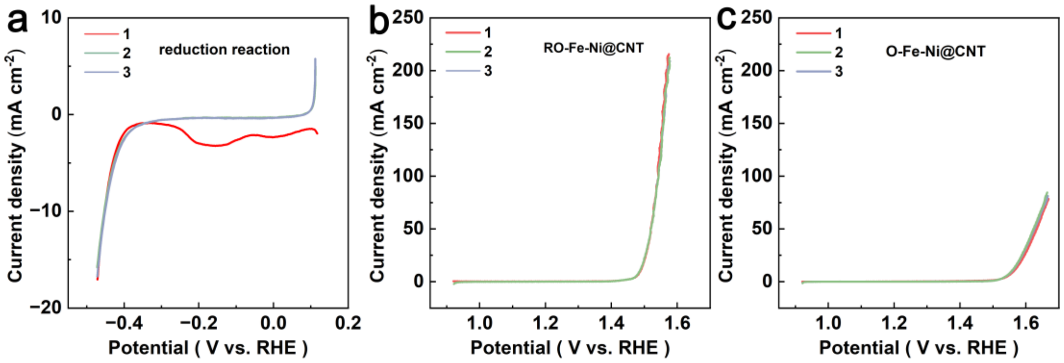

Fig. S15. Linear sweep voltammetry curves of a) the reduction process of Fe-Ni@CNT to prepare the R-Fe-Ni@CNT, b) the oxidation process of R-Fe-Ni@CNT to obtain the RO-Fe-Ni@CNT, and c) the oxidation process of Fe-Ni@CNT to obtain the O-Fe-Ni@CNT, respectively.

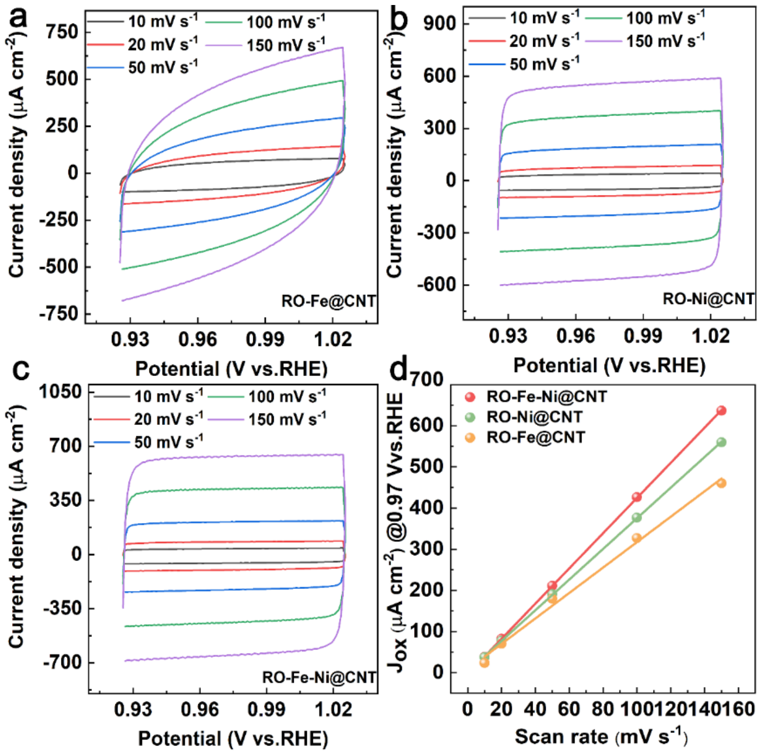

Fig. S16. CV curves of (a) RO-Fe@CNT; (b) RO-Ni@CNT; (c) RO-Fe-Ni@CNT; and (d) linear fitting plots used for evaluating the C_{dl} against the scan rate at 0.97 V vs. RHE.

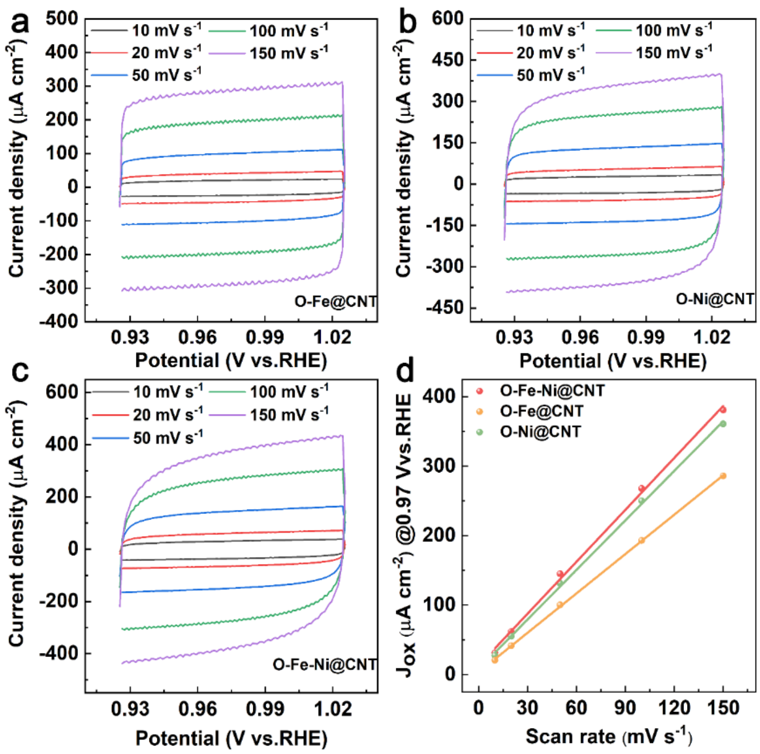

Fig. S17. CV curves of (a) O-Fe @CNT; (b) O- Ni@CNT; (c) O-Fe-Ni@CNT; and (d) linear fitting plots used for evaluating the C_{dl} against the scan rate at 0.97 V vs. RHE.

The electrochemical active surface area of the catalysts was determined through measurements of electrical double-layer capacitance.[14–16] According to Fig. S16d and S17d, the electrical double-layer capacitance could be obtained. Then the electrochemical active surface area could be obtained based on the specific capacitance value of a smooth standard with a real surface area of 1 cm^{-2}.[17] Based on previous studies, 40 μF cm^{-2} is considered the value of specific capacitance for a smooth standard with a real surface area of 1 cm^{-2}.

The electrochemical active surface area could be obtained via the following equation:

$$A_{ECSA} = \frac{The\ electrical\ double-layer\ capacitor}{40}$$

For example:

$$\text{Fe-Ni@CNT: } A_{ECSA} = \frac{4270}{40} = 106.75\ cm^2_{ECSA}$$

Table S6. Calculated electrochemical active surface area (ECSA) of the obtained samples.

Catalysts	Specific Capacitance (μF cm^{-2})	ECSA (cm^2 $_{ECSA}$)
O-Ni-Fe@CNTs	2280	57.00
RO-Fe-Ni@CNTs	4270	106.75
O-Ni@CNTs	2370	59.25
RO-Ni@CNTs	3720	93.00
O-Fe@CNTs	1890	47.25
RO-Fe@CNTs	3090	77.25

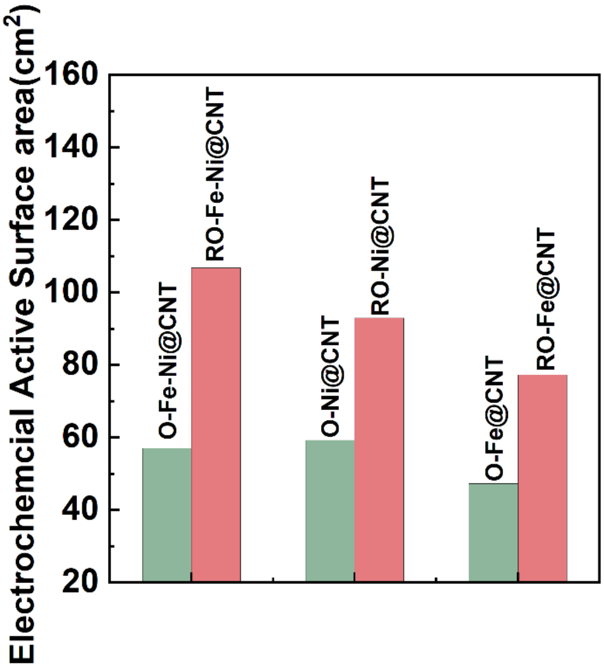

Fig. S18. The bar chart of ECSA for the samples.

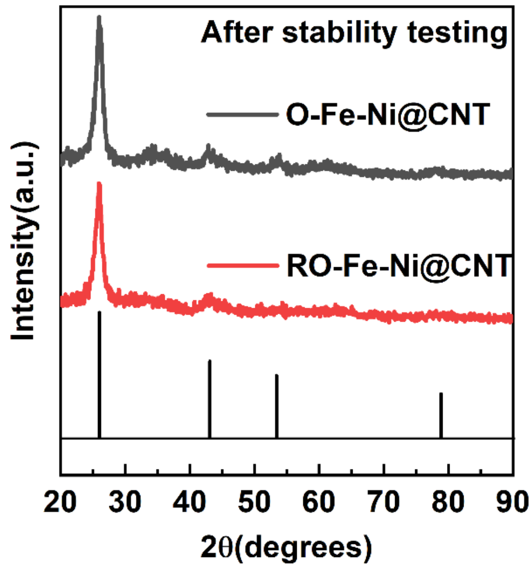

Fig. S19. XRD patterns of the O-Fe-Ni@CNT and RO-Fe-Ni@CNT after the stability testing.

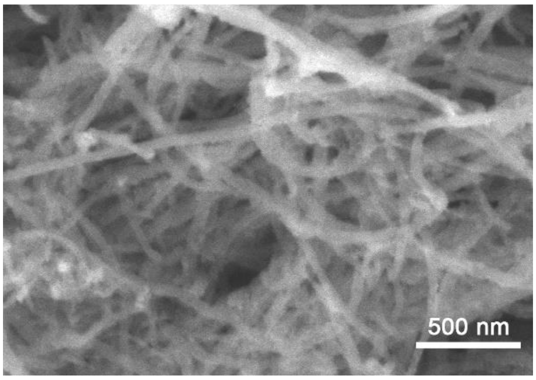

Fig. S20. SEM image of the O-Fe-Ni@CNT after the stability testing.

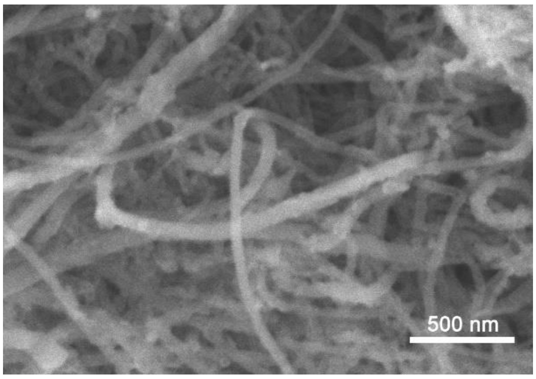

Fig. S21. SEM image of the RO-Fe-Ni@CNT after the stability testing.

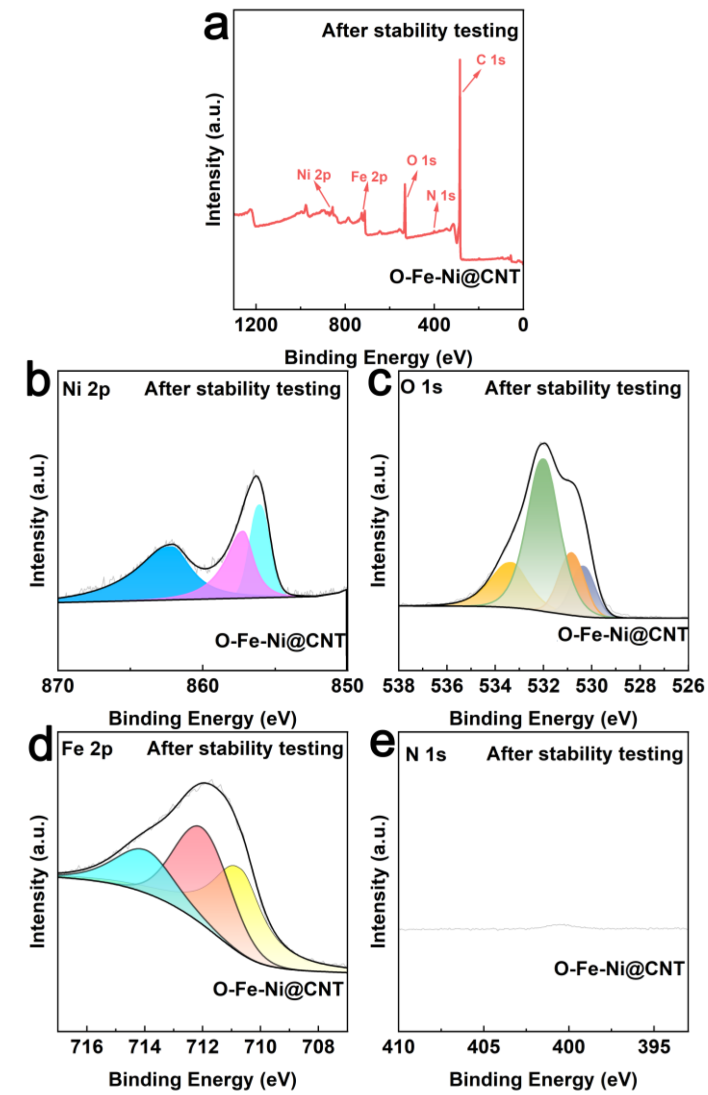

Fig. S22. XPS spectra of the O-Fe-Ni@CNT after the stability testing.

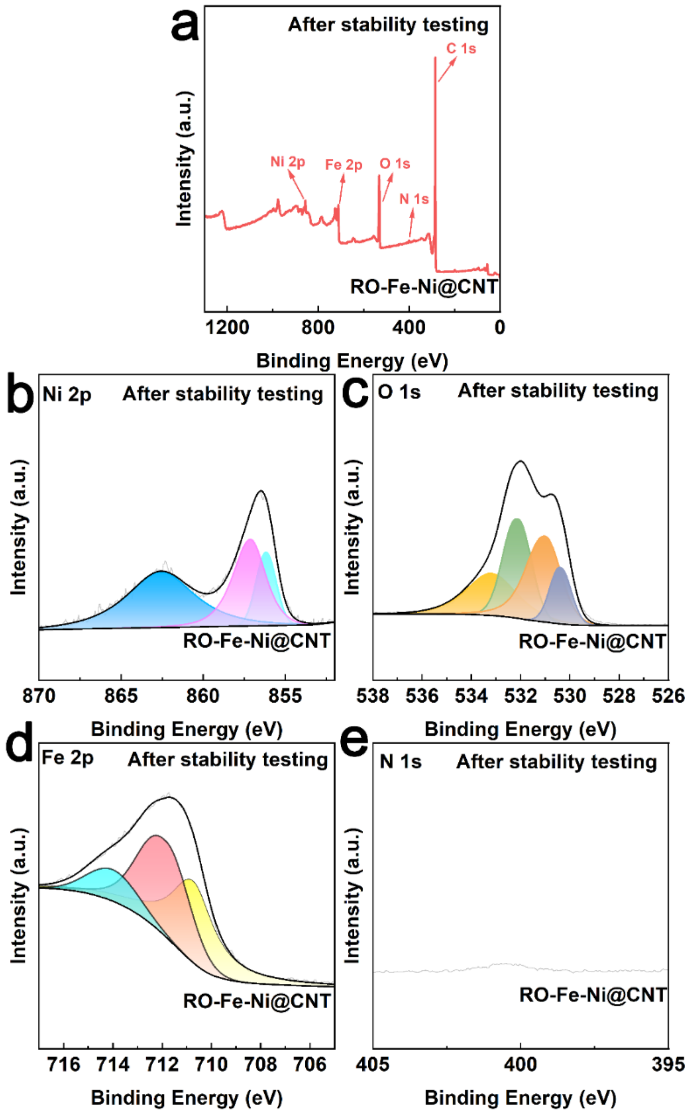

Fig. S23. XPS spectra of the RO-Fe-Ni@CNT after the stability testing.

References

1 B. Ma, Z. Yang, Y. Chen and Z. Yuan, Nickel Cobalt Phosphide with Three-Dimensional Nanostructure as a Highly Efficient Electrocatalyst for Hydrogen Evolution Reaction in Both Acidic and Alkaline Electrolytes. *Nano Res.,* 2019, **12**, 375-380.

2 R. Y. Fan, H. Y. Zhao, Z. Y. Zhao, W. H. Hu, X. Liu, J. F. Yu, H. Hu, Y. M. Chai and B. Dong, Effective Regulation Mechanisms of Fe-Ni(Oxy)Hydroxide: Ni-Rich Heteroatomic Bonding (Ni-O-Fe-O-Ni) Is Essential. *Nano Res.,* 2023, **16**, 12026-12034.

3 C. Ray, S. C. Lee, B. Jin, A. Kundu, J. H. Park and S. C. Jun, Stacked Porous Iron-Doped Nickel Cobalt Phosphide Nanoparticle: An Efficient and Stable Water Splitting Electrocatalyst. *ACS Sustainable Chem. Eng.*, 2018, **6**, 6146-6156.

4 Z. Gao, Z. W. Yu, F. Q. Liu, Y. Yu, X. M. Su, L. Wang, Z. Z. Xu, Y. L. Yang, G. R. Wu, X. F. Feng and F. Luo, Ultralow-Content Iron-Decorated Ni-MOF-74 Fabricated by a Metal-Organic Framework Surface Reaction for Efficient Electrocatalytic Water Oxidation. *Inorg. Chem.,* 2019, **58**, 11500-11507.

5 L. Yu, J. F. Yang, B. Y. Guan, Y. Lu and X. W. (David) Lou, Hierarchical Hollow Nanoprisms Based on Ultrathin Ni-Fe Layered Double Hydroxide Nanosheets with Enhanced Electrocatalytic Activity towards Oxygen Evolution. *Angew. Chem. Int. Ed.*, 2018, **57**, 172.

6 G. Zhou, D. Gao, Y. Dong, L. Wang, H. Wang, X. Wang, V. Linkov and R. Wang, Three-Dimensional Nickel Nanowires Modified by Amorphous Fe Nanosheets as Electrocatalysts for the Oxygen Evolution Reaction. *Dalton Trans.,* 2023, **52**, 5680-5686.

7 F. Zheng, D. Xiang, P. Li, Z. Zhang, C. Du, Z. Zhuang, X. Li and W. Chen, Highly Conductive Bimetallic Ni-Fe Metal Organic Framework as a Novel Electrocatalyst for Water Oxidation. *ACS Sustain. Chem. Eng.,* 2019, **7**, 9743-9749.

8 U. Y. Qazi, C. Z. Yuan, N. Ullah, Y. F. Jiang, M. Imran, A. Zeb, S. J. Zhao, R. Javaid and A. W. Xu, One-Step Growth of Iron-Nickel Bimetallic Nanoparticles on FeNi Alloy Foils: Highly Efficient Advanced Electrodes for the Oxygen Evolution Reaction. *ACS Appl. Mater. Interfaces,* 2017, **9**, 28627-28634.

9 X. Yu, G. Chen, Y. Wang, J. Liu, K. Pei, Y. Zhao, W. You, L. Wang, J. Zhang, L. Xing, J. Ding, G. Ding, M. Wang and R. Che, Hierarchical Coupling Effect in Hollow Ni/$NiFe_2O_4$-CNTs Microsphere via Spray-Drying for Enhanced Oxygen Evolution Electrocatalysis. *Nano Res.,* 2020, **13**, 437-446.

10 J. Jiang, Y. J. Zhang, X. J. Zhu, S. Lu, L. L. Long and J. J. Chen, Nanostructured Metallic FeNi2S4 with Reconstruction to Generate FeNi-Based Oxide as a Highly-Efficient Oxygen Evolution Electrocatalyst. *Nano Energy,* 2021, **81**, 105619.

11 J. H. Kim, D. H. Youn, K. Kawashima, J. Lin, H. Lim and C. B. Mullins, An Active Nanoporous Ni(Fe) OER Electrocatalyst via Selective Dissolution of Cd in Alkaline Media. *Appl. Catal. B Environ.,* 2018, **225**, 1-7.

12 T. Priamushko, P. Guggenberger, A. Mautner, J. Lee, R. Ryoo and F. Kleitz, Enhancing OER Activity of Ni/Co Oxides via Fe/Mn Substitution within Tailored Mesoporous Frameworks. *ACS Appl. Energy Mater.,* 2022, **5**, 13385-13397.

13 J. Lu, W. Hao, X. Wu, X. Shen, S. Cui and W. Shi, Electronic Modulation of the 3D Architectured Ni/Fe Oxyhydroxide Anchored N-Doped Carbon Aerogel with Much Improved OER Activity. *Gels,* 2023, **9**, 190.
14 Y. Sun, Z. Xue, Q. Liu, Y. Jia, Y. Li, K. Liu, Y. Lin, M. Liu, G. Li and C. Y. Su, Modulating Electronic Structure of Metal-Organic Frameworks by Introducing Atomically Dispersed Ru for Efficient Hydrogen Evolution. *Nat. Commun.,* 2021, **12**, 1369.
15 H. Yang, L. Gong, H. Wang, C. Dong, J. Wang, K. Qi, H. Liu, X. Guo and B. Y. Xia, Preparation of Nickel-Iron Hydroxides by Microorganism Corrosion for Efficient Oxygen Evolution. *Nat. Commun.,* 2020, **11**, 5075.
16 Z. Zheng, L. Yu, M. Gao, X. Chen, W. Zhou, C. Ma, L. Wu, J. Zhu, X. Meng, J. Hu, Y. Tu, S. Wu, J. Mao, Z. Tian and D. Deng, Boosting Hydrogen Evolution on MoS_2 via Co-Confining Selenium in Surface and Cobalt in Inner Layer. *Nat. Commun.,* 2020, **11**, 3315.
17 T. Gao, S. Yu, Y. Chen, X. Li, X. Tang, S. Wu, B. He, H. Lan, S. Li, Q. Yue and D. Xiao, Regulating the Thickness of the Carbon Coating Layer in Iron/Carbon Heterostructures to Enhance the Catalytic Performance for Oxygen Evolution Reaction. *J. Colloid Interface Sci.,* 2023, **642**, 120-128.